

imparted into the ISM via shocks is immediately reradiated away, possibly as H_α photons.

23. We have carried out a set of simulations setting different values for the ICM parameters, orientation of the galaxy against the wind, and the composition of the ISM. Two ICM densities have been considered $0.1\rho_{\text{coma}}$ and ρ_{coma} ($\rho_{\text{coma}} = 2.6 \times 10^3 h_{50}^{1/2}$ atoms m^{-3}). The ICM velocities used were 1000 and 2000 km s^{-1} . The orientation of the galaxies moving through the wind were varied from face-on to edge-on, passing through 45° and 20° . We use three ISM compositions: (i) uniform smooth exponential disk (20°). (ii) The previous disk but with a central region devoid of diffuse HI gas with a 2-kpc radius. (iii) The original exponential disk in which 10 small holes each of radius 300 parsecs are randomly located within a 5-kpc radius from the center, and in the same region the local density of the cells is randomly increased by a factor of 2 with a 50% probability. This last case pretends to resemble an inhomogeneous ISM. All of the simulations show a rapid loss of gas but the models with $\rho_{\text{ICM}} = 0.1\rho_{\text{coma}}$, $v_{\text{ICM}} = 1000 \text{ km s}^{-1}$, and no holes, are not able to remove the bulk of this material. Simulations with high ICM velocity and density but with a smooth ICM with no holes retain small HI disk with sizes of 3 kpc after 100 My. The more realistic cases including a nonuniform ISM exhibit massive gas losses with almost no HI component remaining after 100 My. Only the strict edge-on cases are weakly affected by the stripping processes, but this configuration for several orbits is expected to be quite rare. Results of one simulation including 10 small holes and inhomogeneous density are shown as mpeg movies at www.sciencemag.org/feature/data/1050370.shl.

24. Ram pressure stripping removes the outer disk gas in a time scale of 20 My. Turbulence and viscous stripping operate over the entire surface of the disk and are effective at removing the diffuse HI even from regions of the disk that are above the threshold for ram pressure effects. These latter processes operate over a longer time scale and are effective at depleting the diffuse HI from the central disk in a time scale of the order of the crossing time for the ICM through the ISM (Fig. 2).

25. M. R. Merrifield, *Mon. Not. R. Astron. Soc.* **294**, 347 (1998).

26. I. R. Stevens, D. M. Acreman, T. J. Ponman, *Mon. Not. R. Astron. Soc.* **310**, 663 (1999).

27. B. G. Elmegreen and Y. N. Efremov, *Astrophys. J.* **480**, 235 (1997).

28. E. Brinks and E. Bajaja, *Astron. Astrophys.* **169**, 14 (1986).

29. It is important to stress that the process described here can be very effective at modifying galactic morphologies throughout clusters. Following the results in (8) where the average galaxy orbit in clusters was determined, we have estimated that more than 90% of galaxies within a rich virialized cluster can be completely stripped of their diffuse HI. This calculation relied on the facts that: (i) The typical time scale of the stripping is very short compared to the orbital characteristic time of a galaxy in cluster ($\sim 10^8$ years); (ii) even for galaxies moving with a relative angle of 20° to the ICM, all the gas is stripped (Fig. 1); and (iii) the form of the galactic orbits, typically with pericenters < 500 kpc and an average relation apocenter:pericenter approximately 6:1, in clusters and all possible orientations respect the ICM.

30. B. Vollmer, V. Cayatte, A. Boseli, C. Balkowski, W. J. Duschl, *Astron. Astrophys.* **349**, 411 (1999).

31. S. D. Ryder, G. Purcell, D. Davis, V. Anderson, *Publ. Astron. Soc. Aust.* **14**, 1 (1997).

32. Indirect evidence for cluster-galaxy hydrodynamic interactions is frequently observed in head-tail radio galaxies with escaping radio-jets that are stripped backwards by the ICM. This long-lived synchrotron emission may arise within the stripped and subsequently ionized plasma that is in pressure equilibrium with the ICM, supported by the original disk magnetic field that is entangled with the stripped disk material [Web fig. 1 (41)].

33. R. H. Warmels, *Astron. Astrophys. Suppl.* **72**, 57 (1988).

34. V. Cayatte, C. Balkowski, J. H. Van Gorkom, C. Kotanyi, *Astron. J.* **100**, 604 (1990).

35. H. Bravo-Alfaro, V. Cayatte, J. H. van Gorkom, C. Balkowski, *Astron. J.* **119**, 580 (2000).

36. L. Blitz and F. H. Shu, *Astrophys. J.* **238**, 148 (1980).

37. If the lifetimes of dense molecular clouds are as short as 10^7 years, then the decline in the molecular gas content of infalling galaxies is as rapid as the rate of HI removal by the stripping process. Initially, this seems at odds with the observations of J. D. P. Kenney and J. S. Young [*Astrophys. J.* **344**, 171 (1989)], who found that bright HI-deficient spirals in the Virgo cluster contained similar masses of molecular H to counterparts of the same morphological type in the field. This apparently suggests that molecular clouds must have a lifetime that is considerably longer than the stripping time scale. However, we note that this comparison is made at a fixed morphology. Morphology is strongly dependent on the star formation rate, in the sense that galaxies with low star formation rate will be classified as earlier type. Thus, it is unlikely that galaxies with similar morphology will exhibit large differences in CO content. Rather, a large deficiency in CO will result in a galaxy with low star formation rate and earlier morphological type. It is then hard to disen-

tangle any deficiency in CO content due to stripping from the reduction in CO content expected for the change in morphological type. It is encouraging, nevertheless, that galaxies of earlier type match more closely the curve in Kenney and Young's data expected if the molecular and atomic gas contents decline at similar rates.

38. Y. Fujita and M. Nagashima, *Astrophys. J.* **516**, 619 (1999).

39. G. Gavazzi et al., *Astron. Astrophys.* **304**, 325 (1995).

40. J. D. P. Kenney and R. A. Koopmann, *Astron. J.* **117**, 181 (1999).

41. Supplementary material is available at www.sciencemag.org/feature/data/1050370.shl.

42. V.Q. is a Marie Curie research fellow of the European Union (grant HPMF-CT-1999-00052). During the first part of this work, V.Q. was supported by a fellowship of the Spanish SEUID (Ministerio de Educación y Cultura) and partially by Spanish DGES (grant PB96-0797). B.M. is a Royal Society research fellow. Numerical simulations were carried out as part of the Virgo Consortium and the UK Computational Cosmology Consortium.

13 March 2000; accepted 12 April 2000

Photon-Mediated Hybridization of Frenkel Excitons in Organic Semiconductor Microcavities

David G. Lidzey,^{1*} Donal D. C. Bradley,¹ Adam Armitage,[†] Steve Walker,² Maurice S. Skolnick¹

Coherent excitations of intricate assemblies of molecules play an important role in natural photosynthesis. Microcavities are wavelength-dimension artificial structures in which excitations can be made to couple through their mutual interactions with confined photon modes. Results for microcavities containing two spatially separated cyanine dyes are presented here, where simultaneous strong coupling of the excitations of the individual dyes to a single cavity mode leads to new eigenmodes, described as admixtures of all three states. These "hybrid" exciton-photon structures are of potential interest as model systems in which to study energy capture, storage, and transfer among coherently coupled molecular excitations.

The light-harvesting complexes of photosynthetic bacteria act to capture, store, and subsequently funnel energy to the reaction center, where electron transfer then initiates the energy conversion that drives life (1). Such processes are extremely fast and efficient and are believed to involve coherent excitations of intricate assemblies of macrocyclic chromophores. However, the details of their operation are still not fully understood (2). Nature has designed systems in which the three-dimensional structure appears to play a key role in optimizing the individual steps. Optical microcavities, by contrast, are wave-

length-dimensional artificial structures, often less sophisticated in construction, in which excitations can be made to couple through their mutual interaction with confined photon modes. We present microcavity structures in which two remotely separated organic dyes are simultaneously strongly coupled to the same standing-wave optical mode. One may describe this coupled system in terms of a photon-mediated hybridization between the two exciton states. Such devices are of interest in studying coherent Frenkel-exciton coupling. They also bear analogy to the coupled chromophore systems found in nature.

A planar microcavity is a structure that consists of wavelength-thickness semiconductor layers positioned between two mirrors. The cavity quantizes the local electromagnetic field into a discrete set of confined photon modes. If the energy of one of these modes is resonant with an optical transition of the semiconductor, it is possible to modify

¹Department of Physics and Astronomy, Hicks Building, University of Sheffield, Hounsfield Road, Sheffield S3 7RH, UK. ²Department of Electronic and Electrical Engineering, Mappin Street, Sheffield S1 3JD, UK.

*To whom correspondence should be addressed. E-mail: d.g.lidzey@sheffield.ac.uk

[†]Present address: Department of Physics, University of Bath, Claverton Down, Bath BA2 7AY, UK.

the semiconductor absorption and emission characteristics. Microcavities are of both fundamental and practical interest, with potential applications in advanced opto-electronic devices (3–7).

The strength of the coupling between an exciton and a confined photon is categorized as either weak (8) or strong (9–12), depending on whether the Fermi Golden Rule is simply perturbed or no longer holds for the optical transition probabilities. Strong coupling was initially observed in microcavities containing inorganic materials at low temperature (9). However, we recently demonstrated that the strong coupling regime can be readily accessed at room temperature for organic materials (13, 14). In those experiments, a single organic semiconductor was present within the cavity. We now report results for microcavities that contain two spatially separated layers of different organic semiconductors.

Similar interactions have been studied previously within inorganic semiconductor microcavities at low temperature. Results for both the interaction of two different exciton states with a single photon state (15) and of two photon states with a single exciton state (16) have been reported. For a single-cavity photon state interacting with two inorganic exciton states, the maximum energy separation between excitons under which hybridization can occur is limited by their interaction strength with the cavity photon. The typical observed interaction strength is measured by the vacuum Rabi splitting, and in GaAlAs/GaAs quantum well microcavities, it is ≤ 7 meV at 20 K. Thus, Wainstain *et al.* (15) were able to demonstrate hybridization between two GaAlAs/GaAs quantum well exciton states that were separated in energy by $\Delta E = 4$ meV. In this report, we demonstrate that because of the enhanced oscillator strength of Frenkel excitons, hybridization can occur between excitons separated in energy by 60 meV or more at room temperature.

We used two J-aggregate-forming cyanine dyes as the organic semiconductors in our structures (17, 18). The chemical structures of the dyes are shown (insets in Fig. 1, A and B) and are labeled Ex₁ and Ex₂. The relatively narrow transition linewidth (≈ 40 meV) and large oscillator strength typical of J-aggregated dyes are well suited to the observation of strong coupling. We have previously used Ex₁ to demonstrate room-temperature cavity polariton photoluminescence (14). The J aggregates in our devices are dispersed in the polar matrix polymer polyvinyl alcohol (PVA). The absorption spectra for thin film samples of each material are also shown (Fig. 1, A and B).

To ensure that the only coupling that can occur between the two exciton species is that mediated by a cavity photon, the cyanine dye J-aggregate layers were spatially separated by

a 100-nm-thick barrier layer of polystyrene to give an average exciton separation of 140 nm. This precludes short-range dipole-dipole interactions that are characterized by Förster transfer radii of typically less than 10 nm. The absorption of such a multilayer film deposited on a glass substrate (Fig. 1C) shows that $\Delta E \approx 60$ meV, which is comfortably less than the Rabi splittings of 80 meV observed previously in Ex₁-containing single-component microcavities (14).

The generic structure of the microcavities, together with the electric field distribution of the cavity mode, which was simulated using a transfer matrix model, are illustrated (Fig. 1D). Nodes occur at the surfaces of the mirrors, and the field has its maximum in the center of the polystyrene layer. There is, however, a significant field amplitude within each of the cyanine/PVA layers that ensures effective coupling of the photon and exciton modes.

To study the optical properties of our structures, we measured their white light reflectivity spectra (19). The cavity modes appear as sharp dips in the reflectivity spectrum by virtue of their (at least partial) photon character that couples them to the outside world. We used angle tuning to adjust the energy of the cavity photon relative to the

two excitons and thus to control their relative coupling. The energy of the confined photons at an external viewing angle θ is given by $E_{\text{ph}}(\theta) = E_0(1 - \sin^2 \theta/n^2)^{-1/2}$, where E_0 is the photon energy at angle $\theta = 0$ and n is the refractive index of the semiconductor. Here, θ is defined relative to the normal of the cavity surface (see Fig. 1D). The cavities were designed so that at normal incidence the energy of the Ex₁ exciton was some 80 meV greater than that of the cavity photon. As the viewing angle increases, the energy of the cavity photon also increases and therefore approaches resonance with each of the excitons in turn: Ex₁ followed by Ex₂.

In the dispersion curve (Fig. 2A) obtained from the angular variation of the reflectivity spectra for one specific structure, three branches appear with two anti-crossings as expected for a coupled exciton-photon-exciton system. The lower branch of the dispersion curve is visible for all cavity angles, whereas the middle and upper branches can only be detected for angles $> 30^\circ$. At smaller angles (0 to 25°), only the lower branch has significant photon character. As the viewing angle increases, the photon character of the middle and upper branches increases. At $\theta = 30^\circ$, the middle branch possesses a significant photon component and can thus be detected

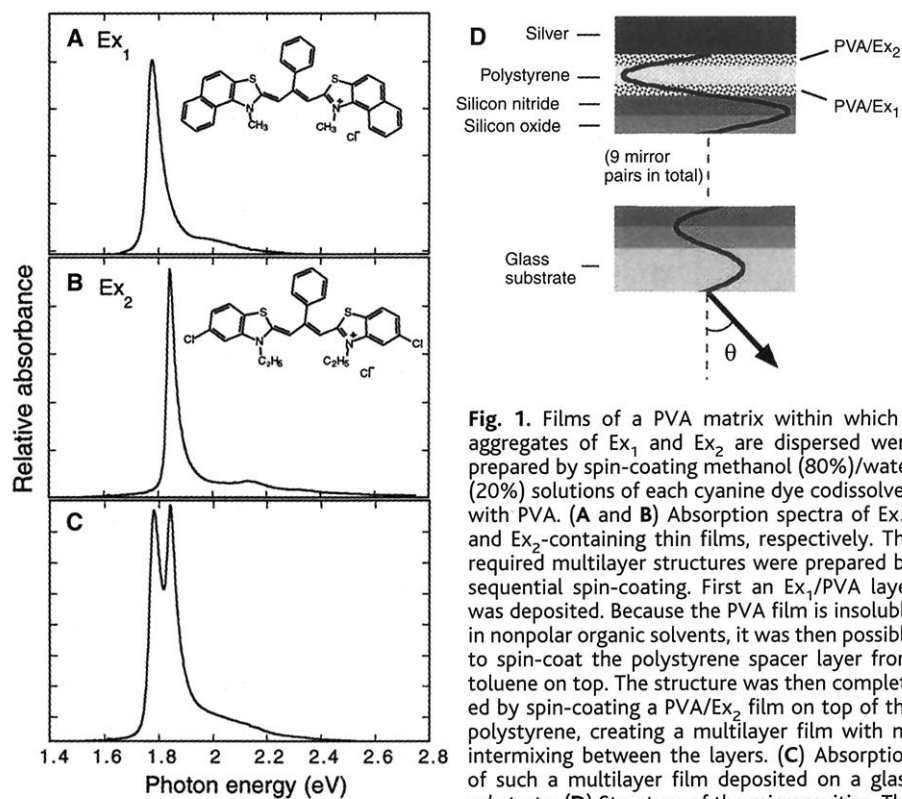


Fig. 1. Films of a PVA matrix within which J aggregates of Ex₁ and Ex₂ are dispersed were prepared by spin-coating methanol (80%)/water (20%) solutions of each cyanine dye codissolved with PVA. (A and B) Absorption spectra of Ex₁- and Ex₂-containing thin films, respectively. The required multilayer structures were prepared by sequential spin-coating. First an Ex₁/PVA layer was deposited. Because the PVA film is insoluble in nonpolar organic solvents, it was then possible to spin-coat the polystyrene spacer layer from toluene on top. The structure was then completed by spin-coating a PVA/Ex₂ film on top of the polystyrene, creating a multilayer film with no intermixing between the layers. (C) Absorption of such a multilayer film deposited on a glass substrate. (D) Structure of the microcavities. The bottom mirror onto which the organic layers were spin-coated was a dielectric mirror consisting of nine alternating $\lambda/4$ layers of SiO₂ and Si_xN_y. The normal incidence reflectivity of the mirror had a peak value of 98% at 1.82 eV. The thickness of each PVA/J-aggregate layer was approximately 40 nm, and the polystyrene barrier layer was 100 nm. This results in a $\lambda/2$ cavity mode (with a normal incidence wavelength of 714 nm, corresponding to a photon energy of 1.74 eV).

in reflectivity. At $\theta = 35^\circ$, the upper branch also possesses a significant photon character and becomes detectable.

We can describe the observed behavior quantitatively using a model based on the interaction of three independent states. Following (16), we describe the compound oscillator made up of the two exciton and one photon modes with the matrix equation

$$\begin{pmatrix} E_{\text{ph}} - E & V_1 & V_2 \\ V_1 & E_{\text{Ex}_1} - E & 0 \\ V_2 & 0 & E_{\text{Ex}_2} - E \end{pmatrix} \begin{pmatrix} \alpha \\ \beta \\ \gamma \end{pmatrix} = 0 \quad (1)$$

Here E_{ph} , E_{Ex_1} , and E_{Ex_2} are the energies of the noninteracting cavity photon, and the two excitons and E are the eigenvalues of the coupled system. V_1 and V_2 are the interaction potentials between the photon and each of the two excitons. α , β , and γ are the coefficients of the basis functions of the bare photon, Ex_1 and Ex_2 , respectively. These coefficients describe the weighting of each of the states in the coupled system. The matrix can be readily diagonalized to obtain the eigenvalues (E) and coefficients (α , β , and γ). To compare with the experimental data, we calculated the photon energy dispersion $E_{\text{ph}}(\theta)$ via a transfer matrix model in which the only free variables are the photon energy at 0° and the refractive index of the cavity. This is then input into the expression for the eigenvalues, and a best fit is obtained to the experimental dispersion by varying E_{Ex_1} , E_{Ex_2} , V_1 , and V_2 but subject to the condition that the energy of each exciton and its interaction potential must remain constant as a function of angle.

The resulting best-fit theoretical dispersions for the polariton branches (Fig. 2A) are compared with the experimental data points. The agreement between the model and the measured data is excellent, demonstrating the applicability of the coupled oscillator model to describe this system. In Fig. 2B, we show the calculated values of $|\alpha|^2$, $|\beta|^2$, and $|\gamma|^2$ for the central branch only. We do not discuss the composition of the upper or lower branches, because they mainly contain contributions from the cavity photon and only one of the two excitons. At small angles, the middle branch is dominated by a contribution from Ex_1 excitons ($|\beta|^2 \approx 0.9$ at 0°). However, as the cavity photon moves closer to the Ex_1 exciton energy, coupling starts to occur with both the photon and Ex_2 excitons. The result is that at 32° , the middle branch contains almost equal contributions from the Ex_1 and Ex_2 excitons and the cavity photon (i.e., $|\alpha|^2 \approx |\beta|^2 \approx |\gamma|^2$). In the reflectivity spectrum measured at an angle of 35° that is close to the point of maximum exciton mixing (Fig. 2C), the three polariton modes are all clearly visible as dips in the reflectivity spectrum. This is consistent with the almost equal dis-

tribution of photon character between the three modes that is calculated.

The interaction strength (Rabi splitting) between the photon and excitons is estimated from the closest approach between the polariton branches. For a cavity containing a cyanine dye concentration of approximately $2.3 \times 10^{20} \text{ cm}^{-3}$, we determine a splitting between the lower and middle branches of 37 meV and between the middle and upper branches of 58 meV. By changing the concentrations of the Ex_1 and Ex_2 dyes in the two active layers, it is possible to change the effective oscillator strengths of the layers and consequently their Rabi-splitting energies (13). In the dispersion curve for a second (otherwise identical) cavity with lower cyanine dye concentration of $1.2 \times 10^{20} \text{ cm}^{-3}$ (Fig. 3A), the shape of the middle branch is

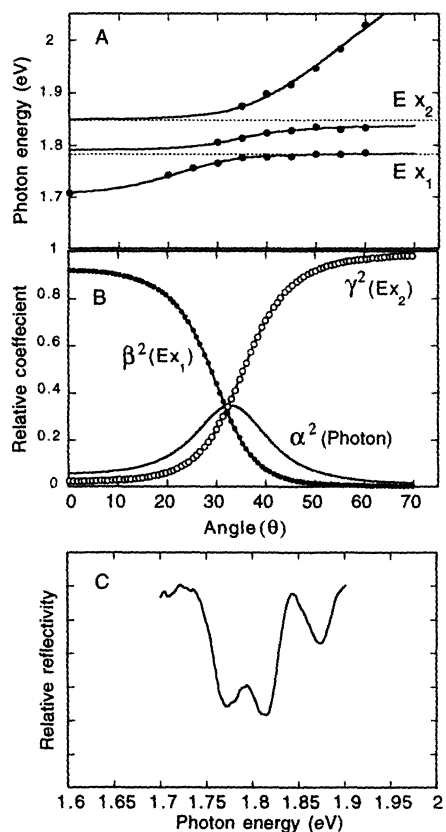


Fig. 2. (A) Dispersion curves obtained from the angular variation of the reflectivity spectra for one specific structure. The solid circles mark the energetic positions of the observed modes. The energies of the two unperturbed exciton transitions are also marked (horizontal dashed lines). The solid lines are the predicted dispersion of the polariton modes determined by solution of Eq. 1. (B) Calculated values of $|\alpha|^2$, $|\beta|^2$, and $|\gamma|^2$ for the middle polariton branch in (A). (C) Reflectivity spectrum measured at an angle of 35° , a point close to maximum exciton mixing. At this angle, the middle branch is calculated to have photon, Ex_1 , and Ex_2 coefficients of $|\alpha|^2 \approx 0.32$, $|\beta|^2 \approx 0.48$, and $|\gamma|^2 \approx 0.18$, respectively.

different from that in Fig. 2A, with a more rapid dispersion as a function of angle. The calculated values of $|\alpha|^2$, $|\beta|^2$, and $|\gamma|^2$ for the middle branch are shown (Fig. 3B). At 43° , the components of Ex_1 and Ex_2 in the mixed mode are $|\beta|^2 \approx |\gamma|^2 \approx 0.15$. We measure a splitting between the middle and lower branch of 18 meV and between the middle and upper branch of 44 meV. Because of the lower oscillator strength of the exciton layers, the interaction between Ex_1 and the photon is now considerably reduced compared to the energy separation (60 meV) between Ex_1 and Ex_2 levels. Thus, the photon cannot significantly couple to both excitons simultaneously. Hence, after interaction with Ex_1 , the middle branch reverts back to being principally photon-like before significant interaction can occur with Ex_2 . The relatively steep gradient of the middle branch (between interaction with the two excitons) occurs because photon-like modes have a much larger dispersion than do exciton-like modes (10). In the re-

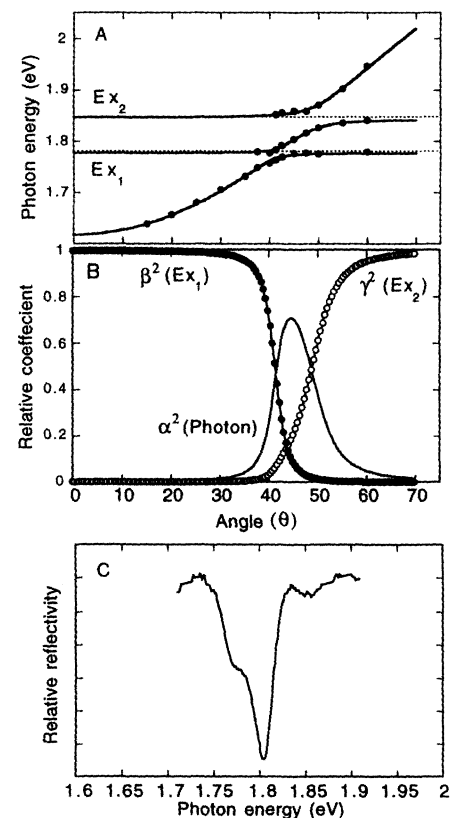


Fig. 3. (A) Dispersion curves for a cavity with lower cyanine dye concentrations. The solid circles mark the energetic positions of the observed modes. The solid lines are the predicted dispersion of the polariton modes. (B) The calculated values of $|\alpha|^2$, $|\beta|^2$, and $|\gamma|^2$ for the middle branch. (C) Reflectivity of the cavity measured at 45° , an angle close to the maximum exciton coupling. At this point, the middle branch is calculated to have photon, Ex_1 , and Ex_2 coefficients of $|\alpha|^2 \approx 0.70$, $|\beta|^2 \approx 0.22$, and $|\gamma|^2 \approx 0.08$, respectively.

flectivity of the cavity measured at 45°, an angle close to the maximum exciton coupling (Fig. 3C), the central mode appears sharper and more intense than either of the other two modes. This is because it is mainly photon-like, and the linewidth of the bare cavity photon is approximately half that of the two bare exciton transitions. These experiments demonstrate the ease of control that is afforded by this system over the relative exciton-photon composition of the central polariton branch.

It is instructive to use the coupled oscillator model to further explore the optical properties of such systems as a function of the exciton-photon interaction strength. Simulating the “visibility” of the cavity polariton modes as a function of the coupling strength V (where $V = V_1 = V_2$) of the two organic exciton components (Fig. 4), it is seen that the visibility of the modes is proportional to the depth of the dips in the experimentally determined reflectivity spectra. In the case of the cavity photon positioned equidistant in energy between the two different excitons (whose unperturbed energies are marked by dotted lines), corresponding to maximum exciton-exciton hybridization in the central

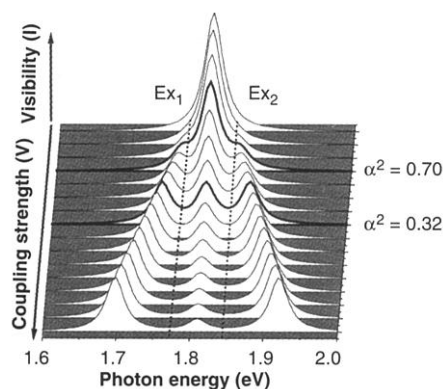


Fig. 4. Simulation of polariton visibility at maximum exciton mixing as a function of the coupling strength V (where $V = V_1 = V_2$) between the two organic exciton components. The visibility of each of the polariton features is proportional to the square of its relative photon component (α). Using Eq. 1, we determine $|\alpha|^2$ and the peak energy E for each of the three polariton modes. We then simulate the cavity visibility spectrum I as a function of photon energy (E_{ph}). The visibility spectrum is constructed from three Lorentzian line shapes, each of height $|\alpha_i|^2$ with central energy E_i , where the subscript i indicates the lower, middle, or upper polariton branches. Thus, for each particular value of V

$$I = \sum_{i=1}^3 \frac{|\alpha_i|^2}{[(E_{ph} - E_i)^2 + (\Delta/2)^2]}$$

where Δ is the linewidth of each branch (each assumed to be 30 meV). For simplicity, we take no account of the (relatively) small changes in linewidth that occur on strong coupling (23). The unperturbed energies of the two exciton species are shown as dashed lines.

polariton branch, it can be seen that as the exciton-photon splitting becomes very much larger than the energy separation between the two exciton species, the central polariton branch reduces significantly in visibility. In the limit where the two spatially separated exciton species have equal energy ($\Delta E = 0$), the central polariton branch has no photon component (20) and is thus termed a dark state (21).

Two spectra are highlighted that have a central-branch photon content of $|\alpha|^2 = 0.32$ and 0.70 (Fig. 4). These correspond to the reflectivity spectra shown in Fig. 2C and 3C, respectively. Slight differences are apparent between the measured and simulated spectra, which may be because the exciton species in the microcavities do not couple to the cavity photon with equal strength (i.e., $V_1 \neq V_2$). There is, however, a good overall qualitative agreement between the theoretical and measured spectra, validating our approach.

We have demonstrated that it is possible to create hybrid exciton species within our microcavities that are composed of coherently coupled excitons. These new hybrid exciton-photon structures are of potential interest as model systems in which to study energy capture, storage, and transfer among coherently coupled molecular excitations. As already noted, both bright and dark states are expected, and these may allow studies of energy capture and storage functions.

It is also interesting to consider whether our structures will permit long-range energy transfer. Wainstain *et al.* (15) performed both resonant and nonresonant excitation of their coupled quantum-well devices but concluded that no significant energy transfer occurred between the upper and lower exciton reservoirs. It is possible that this was the result of a low density of polariton states, combined with the relatively slow rate at which inorganic excitons can populate such states. Whether the same holds true here is yet to be determined, but we note that many of the optical features in our device are similar.

It is significant, however, that unlike previous studies of inorganic semiconductor microcavities, the coupling here survives to room temperature and can hybridize states separated in energy by many tens of meV. We note that there are also differences expected for coherently coupled Frenkel excitons: First, exciton scattering rates might be expected to be significantly enhanced, because Frenkel excitons have large interaction cross-sections with molecular vibrations. Any energy transfer from Ex_2 to Ex_1 would require the dissipation of some 60 meV per polariton. Raman spectroscopy of Ex_2 J-aggregates shows that there is a vibrational mode with an energy of 74 meV. This might be a suitable energy loss channel. Second, it

is possible to conceive of organic multilayer structures in which the upper exciton reservoir alone could be excited. In this case, quite small amounts of energy transfer to the lower polariton branch might be detectable. Constructing and evaluating such devices will be technologically challenging; however, if energy transfer does prove possible, there will be strong interest in this and related systems for a variety of optoelectronic device structures, including the postulated Frenkel-Wannier hybrid exciton devices (22).

References and Notes

- X. Hu and K. Schulten, *Phys. Today* **50** (no. 8), 28 (1997).
- G. R. Fleming and R. van Grondelle, *Phys. Today* **47** (no. 2), 48 (1994).
- For example, see J. Jewell, *Phys. World* **1990**, 28 (July 1990).
- M. S. Ünlü and S. Strite, *J. Appl. Phys.* **78**, 607 (1995).
- P. K. H. Ho, D. S. Thomas, R. H. Friend, N. Tessler, *Science* **285**, 233 (1999).
- N. Tessler, G. J. Denton, R. H. Friend, *Nature* **382**, 695 (1996).
- D. G. Lidzey, D. D. C. Bradley, S. J. Martin, M. A. Pate, *IEEE J. Sel. Top. Quant. Electron.* **4**, 113 (1998).
- D. G. Lidzey *et al.*, *Appl. Phys. Lett.* **71**, 744 (1997).
- C. Weisbuch, M. Nishioka, A. Ishikawa, Y. Arakawa, *Phys. Rev. Lett.* **69**, 3314 (1992).
- M. S. Skolnick, T. A. Fisher, D. M. Whittaker, *Semicond. Sci. Technol.* **13**, 645 (1998).
- T. B. Norris, *Confined Electrons and Photons*, E. Burstein and C. Weisbuch, Eds. (Plenum, New York, 1995).
- P. Senellart and J. Bloch, *Phys. Rev. Lett.* **82**, 1233 (1999).
- D. G. Lidzey *et al.*, *Nature* **395**, 53 (1998).
- D. G. Lidzey, D. D. C. Bradley, T. Virgili, A. Armitage, M. S. Skolnick, *Phys. Rev. Lett.* **82**, 3316 (1999).
- J. Wainstain *et al.*, *Phys. Rev. B* **58**, 7269 (1998).
- A. Armitage *et al.*, *Phys. Rev. B* **58**, 15367 (1998).
- E. O. Potma and D. A. Wiersma, *J. Chem. Phys.* **108**, 4894 (1998).
- D. Möbius, *Adv. Mater.* **7**, 437 (1995).
- D. Baxter *et al.*, *Phys. Rev.* **B56**, R10032 (1997).
- The appearance of dark states can be demonstrated analytically. For the case of two excitons of equal energy, resonant with a cavity photon ($E_{Ex_1} = E_{Ex_2} = E_{ph} = \epsilon$), Eq. 1 can be rewritten

$$\begin{pmatrix} \epsilon - E & V & V \\ V & \epsilon - E & 0 \\ V & 0 & \epsilon - E \end{pmatrix} \begin{pmatrix} \alpha \\ \beta \\ \gamma \end{pmatrix} = 0$$

For simplicity, we consider the case of equal coupling between the excitons and cavity photon ($V_1 = V_2 = V$). By diagonalizing the Hamiltonian, it can be shown that the roots of the equation have energy $E = \epsilon$ (the central polariton branch), and $E = \epsilon \pm V\sqrt{2}$ (the upper and lower polariton branches). Using the fact that $\alpha^2 + \beta^2 + \gamma^2 = 1$, it can then be shown that the central branch has basis function weightings of $\alpha = 0$, $\beta = \gamma = 1/\sqrt{2}$. The upper and lower branches have weightings of $\alpha = 1/\sqrt{2}$, $\beta = \gamma = 1/2$. Thus, on resonance, the cavity photon is equally distributed between the upper and lower branches and has no component in the middle branch (rendering it dark).

- V. M. Agranovich, G. C. La Rocca, F. Bassani, *Phys. Status Solidi A* **164**, 39 (1997).
- V. Agranovich, H. Benisty, C. Weisbuch, *Solid State Commun.* **102**, 631 (1997).
- Y. Zhu *et al.*, *Phys. Rev. Lett.* **64**, 2499 (1990).
- We gratefully acknowledge the United Kingdom Engineering and Physical Sciences Research Council for their support of this work through research grant GR/L01916 and through an Advanced Fellowship award to D.G.L. We also thank T. Virgili and M. Ariu for Raman measurements and V. Agranovich for very fruitful discussions.

6 March 2000; accepted 5 April 2000